Research Square

Preprints are preliminary reports that have not undergone peer review.
They should not be considered conclusive, used to inform clinical practice,
or referenced by the media as validated information.

Three-dimensional volumetric characterization of CFRP surface integrity in milling: comparison with conventional roughness parameters

Anh Tuan Dang
Thai Nguyen University of Technology
Van Chec Nguyen
Thai Nguyen University of Technology
Gunasilan Manar
National Defence University of Malaysia: Universiti Pertahanan Nasional Malaysia
Ngọc Nguyễn Đình
ngocnd@tnut.edu.vn

Thai Nguyen University of Technology

Research Article

Keywords: CFRP milling, Above and Below Surface Volume, Three-dimensional surface topography, Surface roughness

Posted Date: November 9th, 2026

DOI: https://doi.org/10.21203/rs.3.rs-11169251/v1

License: This work is licensed under a Creative Commons Attribution 4.0 International License.
Read Full License

Three-dimensional volumetric characterization of CFRP surface integrity in milling: comparison with conventional roughness parameters

Anh Tuan Dang[1], Van Chec Nguyen[2], Gunasilan Manar[3], Dinh Ngoc Nguyen[1*]

1. Faculty of International Training, Thai Nguyen University of Technology, Thai Nguyen, Vietnam

2. Faculty of Mechanical Engineering, Thai Nguyen University of Technology, Thai Nguyen, Vietnam

3. Department of Aeronautical Engineering and Aviation, National Defence University of Malaysia, Kuala Lumpur, Malaysia

Corresponding author: ngocnd@tnut.edu.vn

ORCID:

Dinh Ngoc Nguyen: https://orcid.org/0000-0002-0631-0961;

Anh Tuan Dang: https://orcid.org/0000-0001-6237-6634

Acknowledgments: The authors wish to thank Thai Nguyen University of Technology for supporting this work.

Abstract:

Machined surface quality in carbon fibre reinforced polymer (CFRP) is commonly assessed using roughness parameters, which may not fully represent heterogeneous three-dimensional topography. This study investigates whether volumetric descriptors complement profile and areal roughness in milled CFRP surfaces. Dry up-milling experiments were conducted using a two-flute polycrystalline diamond end mill under a full factorial design with cutting speeds of 200 and 300 m/min and feed per tooth values of 0.017, 0.033 and 0.050 mm/tooth. Surface quality was characterized by focus-variation optical metrology using Ra, Sa, Above Surface Volume and Below Surface Volume. Cutting force, final cutting-edge radius and selected μCT observations supported interpretation of the machining response. Two-way ANOVA showed that feed per tooth accounted for 84.1% of Ra variation, while cutting speed and its interaction with feed were not significant. In contrast, Sa and both volumetric descriptors were significantly affected by cutting speed, feed and their interaction. At 0.050 mm/tooth, increasing cutting speed from 200 to 300 m/min changed Ra only from 1.527 to 1.426 μm, whereas the response shifted from above-surface dominated (V_{above} = 0.975 mm³, V_{below} = 0.033 mm³) to below-surface dominated (V_{above} = 0.106 mm³, V_{below} = 0.231 mm³). The 300 m/min condition exhibited more numerous and extensive μCT-visible discontinuities than the 200 m/min condition. Analysis over cumulative cutting length showed no universal monotonic relationship between cutting force and surface quality. Overall, the separated volumetric descriptors complement Ra and Sa by retaining the direction of three-dimensional topographic deviation, providing additional information for CFRP machining-quality assessment.

Keywords: CFRP milling; Above and Below Surface Volume; Three-dimensional surface topography; Surface roughness

1. Introduction

Carbon fiber reinforced polymer (CFRP) composites are increasingly employed in aerospace, automotive, marine and other high-performance engineering applications because of their high specific strength, high specific stiffness and excellent fatigue performance [1], [2], [3]. Although CFRP components can be manufactured close to their final geometry, secondary machining operations such as milling and drilling are commonly required to achieve the dimensional accuracy, geometrical features and assembly requirements of finished components [4], [5]. However, the heterogeneous and anisotropic nature of CFRP, arising from the combination of stiff carbon fibres, a polymer matrix and fibre–matrix interfaces, makes material removal fundamentally different from conventional machining of metallic materials [6], [7]. Material removal is accompanied by brittle fracture, fibre breakage, fibre pull-out and matrix removal, while the abrasive nature of carbon fibres can accelerate cutting-tool degradation [8], [9], [10]. Consequently, machining conditions and tool condition can strongly influence cutting forces, tool wear and the integrity of the machined surface, making the reliable characterization of machining quality an important issue in the manufacturing of CFRP components [11], [12].

Surface quality is therefore one of the key indicators used to evaluate the performance of CFRP machining. Conventional profile roughness parameters, particularly Ra, and more recently areal parameters such as Sa, have been extensively employed to quantify the geometric quality of machined surfaces and to investigate the effects of cutting parameters, tool geometry and tool wear [13], [14]. For example, recent CFRP milling studies have demonstrated that changes in cutting speed, milling strategy, fibre cutting angle and tool condition can produce measurable variations in

cutting force and areal surface roughness [15], [16]. However, the machined surface of CFRP is inherently heterogeneous and may contain localized fibre fracture, fibre pull-out, matrix removal, burrs, pits, cracks and other irregular features that are not necessarily represented adequately by a single statistical roughness parameter [17], [18], [19]. Recent investigations of CFRP machining have consequently moved toward more detailed characterization of surface morphology and areal topography, while also considering the relationships among surface roughness, cutting force and tool wear. These developments suggest that conventional roughness parameters remain essential for benchmarking machining quality, but complementary descriptors capable of quantifying the magnitude and spatial characteristics of machining-induced surface features may provide additional information for a more comprehensive assessment of CFRP machined surfaces [20], [21], [22].

To overcome some of these limitations, three-dimensional surface topography and areal surface characterization have increasingly been adopted for the assessment of machined CFRP surfaces. In contrast to profile-based parameters, areal measurements provide spatially distributed information over a measured surface and allow localized peaks, valleys and machining-induced defects to be considered. For example, Cai et al. [23] investigated the three-dimensional surface topography of milled CFRP and demonstrated that fibre orientation strongly influences the morphology and roughness of the machined surface. More recently, systematic analyses of CFRP machined surfaces have employed multiple areal parameters, including S_a, S_q, S_{sk}, $S_{ku}$and S_z, to distinguish the effects of fibre orientation and machining conditions on surface morphology [24]. Such approaches represent an important development from conventional two-dimensional roughness measurements because they capture the spatial distribution and statistical characteristics of surface features rather than reducing the surface to a single profile. Nevertheless, most three-dimensional approaches still describe surface quality primarily through height-based or distribution-based roughness parameters, leaving the actual volumetric magnitude of localized material removal and surface defects less explicitly quantified.

A further step toward quantifying machining-induced surface damage is to characterize the volume associated with localized surface defects [25], [26], [27]. In an early and particularly relevant study, Nguyen-Dinh et al. [28] combined scanning electron microscopy, X-ray tomography and three-dimensional optical topography to characterize machining damage generated during CFRP trimming. Rather than relying solely on conventional roughness parameters, the authors proposed crater volume (C_v) and maximum depth of damage as descriptors of machining-induced surface damage and showed that these parameters provided a more realistic representation of the damage than classical roughness criteria when related to the compressive strength of the machined specimens. In a related study, the same research direction further demonstrated that crater volume could be compared with S_a and X-ray tomography observations to characterize the effects of textured surface on the mechanical behavior of CFRP structures [27]. These studies established an important basis for volumetric characterization of CFRP machining damage. However, subsequent CFRP machining studies have continued to rely predominantly on profile or areal roughness parameters, while the volumetric description of machined-surface features has received considerably less systematic investigation. In particular, the potential distinction between material volumes located above and below the reference surface, and how these volumetric components respond to cutting conditions and relate to conventional roughness and machining mechanics, remains insufficiently explored [4], [29] .

Despite these developments, several aspects of volumetric characterization of CFRP machined surfaces remain insufficiently understood. First, although crater volume has been introduced as a descriptor of machining-induced damage, volumetric characterization has not been developed to the same extent as profile- and areal-roughness-based approaches [18], [30]. In particular, the possibility of distinguishing material volume located above and below a reference surface has received limited systematic attention, even though these two components may represent different morphological consequences of the material-removal process. Second, the relationship between volumetric surface descriptors and conventional quality indicators has not been sufficiently established. Recent studies have increasingly investigated the coupled effects of tool wear, cutting force and areal surface roughness [31], while studies of subsurface damage have demonstrated that tool-edge rounding and cutting conditions can substantially affect damage depth [32] . However, these studies have generally treated roughness, force, tool wear and damage as separate or complementary responses rather than examining whether volumetric descriptors can provide additional information linking machining mechanics to the resulting three-dimensional surface morphology. Third, it remains unclear whether volumetric descriptors provide information that is genuinely complementary to conventional roughness and machining-mechanics indicators, or whether they simply reproduce trends already captured by Ra, Sa, or cutting force. Establishing these relationships is necessary to clarify the practical value of volumetric characterization for CFRP machining.

To address these gaps, this study aims to evaluate a volumetric-based approach for characterizing the machining quality of CFRP surfaces and to determine whether volumetric descriptors provide information complementary to conventional roughness parameters. CFRP milling experiments were conducted at two cutting speeds ($V_c = 200$ and 300m/min) and three feed-per-tooth levels ($f_z = 0.017$, 0.033 and 0.050 mm/tooth), while the radial depth of cut was maintained at 2 mm. For each cutting condition, cutting force and three-dimensional surface measurements were obtained, including profile roughness (Ra), areal roughness (Sa), above-surface volume, below-surface volume and projected area. Statistical analyses were performed to quantify the effects of cutting parameters and their interaction

and to examine the relationships among cutting force, conventional roughness and volumetric descriptors. Optical surface observations and a representative transverse profile were additionally used to illustrate selected differences in surface topography, while final cutting-edge measurements were used to support interpretation of the mechanical machining response. For the two high-feed conditions exhibiting the clearest inversion in volumetric response, selected X-ray micro-computed tomography (μCT) observations were additionally obtained at a common subsurface depth to provide independent qualitative evidence for the physical relevance of the Below Surface Volume. The study therefore seeks to establish whether volumetric characterization can reveal machining-induced surface features that are not fully represented by conventional roughness parameters and to provide a more physically informative framework for assessing CFRP machining quality.

The main contributions of this study are threefold. First, it systematically evaluates separated above- and below-surface volumetric responses of CFRP machined surfaces under different combinations of cutting speed and feed per tooth, extending volumetric characterization beyond a single total or crater-volume descriptor. Second, it quantitatively compares the volumetric descriptors with conventional profile roughness Ra, areal roughness Sa, and cutting force to determine whether they provide complementary information for machining-quality assessment. Third, it examines the evolution of these descriptors with cumulative cutting length and verifies the robustness of the volumetric response through normalization by projected area, thereby establishing whether the observed trends reflect genuine changes in three-dimensional topography rather than differences in the analyzed surface area.

2. Experimental procedure

The CFRP plates were prepared from P2352 prepregs with a symmetric stacking configuration of [90°/90°/-45°/0°/45°/90°/-45°/90°/45°/90°]s resulting in plates with a nominal size of 300 mm × 300 mm × 5.2 mm. The mechanical properties of the composite material are summarized in Table 1. Prior to machining, the plates were cut into specimens measuring 270 mm × 16 mm × 5.2 mm. This geometry provided a sufficiently long and accessible machined surface for sequential machining and subsequent surface characterization. Each specimen was machined on both longitudinal faces. After machining one face, the specimen was removed from the fixture, reversed, and subsequently mounted for machining of the opposite face. An unmachined balancing specimen of the same geometry as the test specimen was positioned on the opposite side of the clamping bar to balance the tightening force and maintain repeatable clamping conditions. The overall fixture arrangement is illustrated in Figure 1. Further details regarding the fixture configuration and specimen mounting procedure can be found in [33].

The machining experiments were performed on a Mazak VERTICAL CENTER SMART 530C. Cutting forces were monitored using a Kistler quartz three-component dynamometer (Model 9257BA, Kistler Instruments (Pte) Ltd, Midview, Singapore). For each machined face, the reported cutting-force value was obtained by averaging five measurement positions along the cutting path. These five positions were used to characterize the within-face force response and were not treated as independent experimental replicates. The experimental design comprised two levels of cutting speed and three levels of feed per tooth, while the radial depth of cut, (a_e), was maintained at 2 mm for all cutting conditions. The complete set of machining conditions is provided in Table 2. A new PCD helical end mill was employed for each machining condition. The cutter had two flutes and a diameter of 8 mm, and its geometry is presented in Figure 2. For each combination of cutting parameters, eight toolpaths were performed. Surface characterization was performed at the midpoint of each successive 270-mm machined face, corresponding to cumulative cutting lengths of 0.135, 0.405, 0.675, 0.945, 1.215, 1.485, 1.755 and 2.025 m. Since the length of each machined face was 270 mm, the resulting accumulated cutting length for each machining condition was 2160 mm (270 mm × 8). Four specimens were machined for each cutting condition, and both longitudinal faces of each specimen were machined, yielding eight machined faces per condition. The two faces from the same specimen were treated as paired measurements rather than independent experimental replicates. For the two-way ANOVA, the two face measurements were averaged for each specimen, resulting in four independent specimen-level observations per cutting condition. All experiments were conducted under dry machining conditions using an up-milling configuration.

The machined surfaces were characterized using an Alicona InfiniteFocus optical 3D measurement system. Surface measurements were acquired using a 10× objective, with a vertical resolution of 0.10 μm and a lateral resolution below 8.01 μm. For each specimen, a rectangular region of interest (ROI), with a nominal area of approximately 45 mm², was selected entirely within the machined surface. The two free edges of the specimen, where fraying and protruding fibres commonly occur, were excluded from the ROI to minimize the influence of edge-related damage on the measurement results. The three-dimensional surface roughness was characterized using the areal roughness parameter (S_a) through the SurfaceTextureMeasurement function. In addition, the profile roughness (R_a) was determined from profiles extracted within the same measurement region using a cut-off wavelength of $\lambda_c = 800\mu m$. The Alicona system was also used to characterize the three-dimensional surface topography and cutting-edge geometry.

To quantify the volumetric characteristics of the machined surfaces, the VolumeMeasurement function was employed to determine the topographic volumes located above and below the reference surface, denoted as Above Surface Volume (V_{above}) and Below Surface Volume (V_{below}), respectively. The actual area of the region used for the volumetric

calculation was obtained from the Projected Area parameter provided by the software. For each machined surface, the volumetric measurement was repeated three times within the same optical field without repositioning the specimen on the Alicona stage. The ROI was redefined for each repetition and could vary slightly in position and projected area while remaining within the same machined region. These repeated measurements were used to assess the repeatability of the volumetric characterization rather than as independent experimental replicates. The volume calculation was performed using the Soap Film method, in which an ISO-surface was constructed from the three-dimensional boundary of the selected ROI and used as the reference surface for volume determination. According to the Alicona documentation [34], the Soap Film method generates a bounding surface analogous to a soap film stretched across the three-dimensional boundary of the selected region, allowing the reference surface to adapt to the local geometry rather than being constrained by an absolute planar reference. The Above Surface Volume (V_{above}) and Below Surface Volume (V_{below}) were then calculated as the topographic volumes located above and below this reconstructed reference surface, respectively. This approach has been employed in previous studies [35], [36] to quantify wear or material-loss volumes from three-dimensional topography data, while volumetric profilometry using Alicona systems has also been applied to characterize surface cavities and fibre pull-out in machined CFRP surfaces. Selected specimens were additionally examined by X-ray micro-computed tomography (μCT) using a ZEISS Xradia Versa 620 X-ray Microscope (ZEISS, Germany). The measurements were acquired using a 10× objective, with a reconstructed voxel size of 1.08 μm. The X-ray source was operated at 60 kV and 6.5 W, with 1601 projections acquired over 360°. Reconstructed μCT slices for the two high-feed conditions, $V_c = 200$ and 300 m/min at $f_z = 0.05$mm/tooth, were extracted at the same depth of 100 μm below the machined surface. These μCT observations were used only as qualitative support for the interpretation of the below-surface volumetric response.

The effects of cutting speed, feed per tooth and their interaction on F_t, Ra, Sa, $V_{\text{above}}$and V_{below}were evaluated using two-way ANOVA at a significance level of $p < 0.05$. For the ANOVA, the two machined faces of each specimen were averaged, resulting in four independent specimen-level observations per machining condition. Percentage contributions were calculated from the corresponding ANOVA sums of squares.

Pearson correlation analysis was used to examine the relationships among cutting force and the surface descriptors using the 48 machined-face observations. Additional within-condition correlations were evaluated after subtracting the corresponding cutting-condition means. Linear trends with cumulative cutting length were also examined for each machining condition to characterize the progression of the measured responses.

Table 1. Mechanical properties of P2352 prepreg.

Density (g/cm^3)	Longitudinal shear modulus (GPa)	Longitudinal Young's modulus (GPa)	Compressive strength (MPa)	Tensile strength (MPa)	Poisson's ratio
2.63	6.21	162	1552	2844	0.34

Table 2. Machining parameters

Cutting speed, Vc (m/min)	200 and 300
Feed per tooth, f_z (mm/tooth)	0.017, 0.033, and 0.05

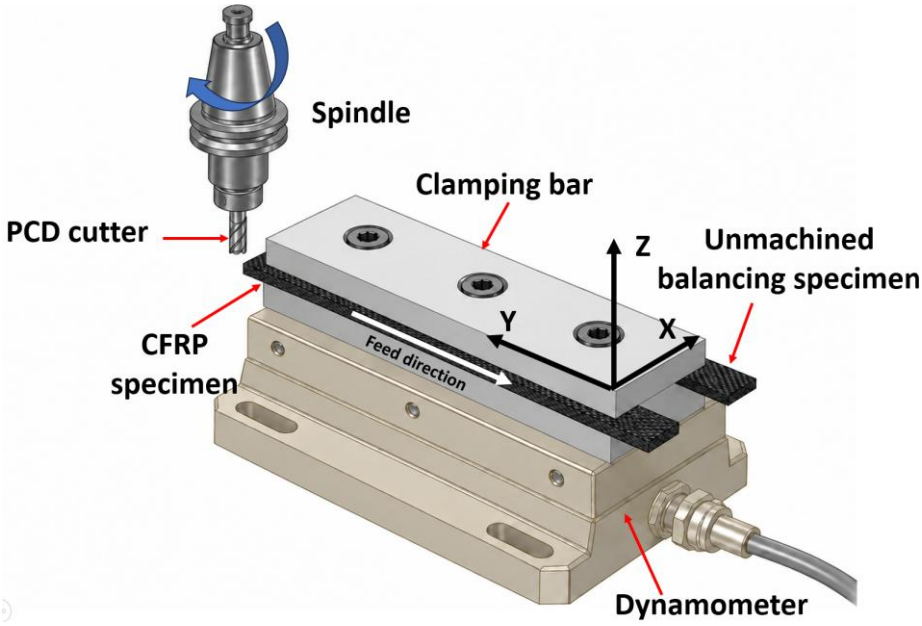


Fig. 1. Schematic illustration of the experimental machining setup used in the present study.

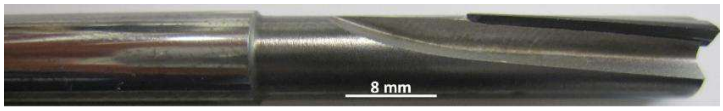


Fig. 2. PCD milling cutter with two helical cutting edges.

3. Results and Discussion

3.1. Cutting force and tool-edge condition

In this research, the resultant cutting force, (F_R), was calculated from the three orthogonal cutting-force components using Eq. (1):

$$F_R = \sqrt{F_x^2 + F_y^2 + F_z^2} \tag{1}$$

where F_x, F_y, F_z denote the feed, normal, and thrust force components, respectively. The corresponding force directions and coordinate system are schematically illustrated in Figure 1.

The resultant cutting force, F_R, was strongly influenced by both cutting speed and feed per tooth. At $V_c = 200$m/min, the mean cutting force increased from 35.64 N at $f_z = 0.017$mm/tooth to 51.66 N at $f_z = 0.033$mm/tooth and reached 72.75 N at $f_z = 0.05$mm/tooth. A similar feed-dependent increase was observed at $V_c = 300$m/min, although the force levels were substantially lower, increasing from 28.49 to 32.64 and 41.27 N over the same feed per tooth range (Fig. 3).

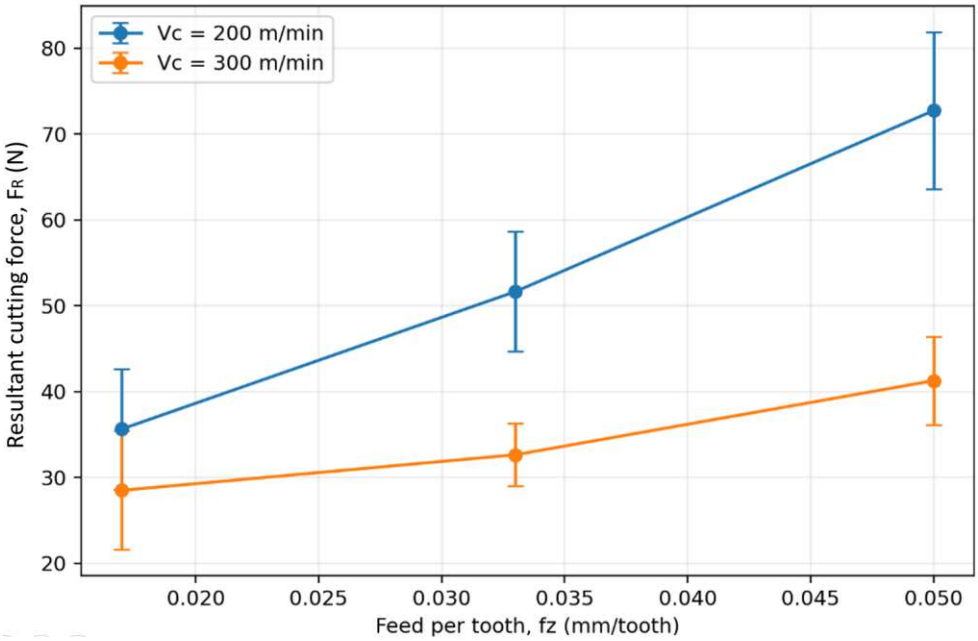


Fig. 3. *Effect of cutting speed and feed per tooth on the cutting force, F_R.*

The statistical effects of cutting speed and feed per tooth on the cutting-force and surface-quality responses were evaluated using two-way ANOVA, and the results are summarized in Table 3. This table provides the common statistical basis for the analyses presented throughout Sections 3.1–3.5. For F_R, both cutting speed and feed per tooth were highly significant, contributing 38.96% and 44.33% of the total variation, respectively, while their interaction contributed 10.42%. The model explained 93.70% of the total variation in cutting force.

Table 3. Two-way ANOVA for cutting force and surface-quality descriptors

Response	Model R^2(%)	Factor	F-value	p-value	Contribution (%)	Significance
F_R	93.70	Cutting speed V_c	111.41	3.87×10^{-9}	38.96	Significant
		Feed per tooth f_z	63.37	7.12×10^{-9}	44.33	Significant
		$V_c \times f_z$	14.89	1.53×10^{-4}	10.42	Significant
Ra	87.82	Cutting speed V_c	0.47	0.501	0.32	Not significant
		Feed per tooth f_z	62.16	8.28×10^{-9}	84.10	Significant
		$V_c \times f_z$	2.51	0.109	3.40	Not significant
Sa	95.14	Cutting speed V_c	45.95	2.38×10^{-6}	12.41	Significant
		Feed per tooth f_z	114.14	5.95×10^{-11}	61.65	Significant
		$V_c \times f_z$	39.03	2.85×10^{-7}	21.08	Significant
V_{above}	95.58	Cutting speed V_c	101.11	8.21×10^{-9}	24.84	Significant
		Feed per tooth f_z	77.76	1.39×10^{-9}	38.21	Significant
		$V_c \times f_z$	66.19	5.04×10^{-9}	32.53	Significant
V_{below}	94.58	Cutting speed V_c	126.96	1.38×10^{-9}	38.26	Significant

		Feed per tooth f_z	52.78	2.96×10^{-8}	31.81	Significant
		$V_c \times f_z$	40.64	2.11×10^{-7}	24.50	Significant

Note: Statistical significance was assessed at $p < 0.05$. Percentage contribution was calculated from the sum of squares of each ANOVA term relative to the total ANOVA sum of squares. The analysis was performed using specimen-averaged data, with the two machined faces of each specimen averaged before ANOVA ($n = 4$ independent specimens per machining condition).

The increase in force with feed per tooth can be attributed to the larger undeformed chip thickness and the consequently greater mechanical resistance to fibre fracture and material removal. Conversely, increasing the cutting speed from 200 to 300 m/min consistently reduced F_R at all feed levels. The magnitude of this reduction depended on feed per tooth and was particularly pronounced at $f_z = 0.05$mm/tooth, where the mean force decreased from 72.75 to 41.27 N. This trend is consistent with previous observations in CFRP milling [33]. The final cutting-edge radius, which was measured using the Alicona system, also varied systematically with the cutting parameters. At $V_c = 200$m/min, the measured edge radius decreased from 12.98μm at $f_z = 0.017$mm/tooth to 11.63μm at $f_z = 0.033$mm/tooth and 9.19μm at $f_z = 0.05$mm/tooth. At $V_c = 300$m/min, the corresponding values were 10.64, 8.95 and 8.61 μm, respectively (Figure 4). Thus, at a fixed feed per tooth, the final edge radius was smaller at the higher cutting speed, while at a fixed cutting speed the radius decreased as feed per tooth increased.

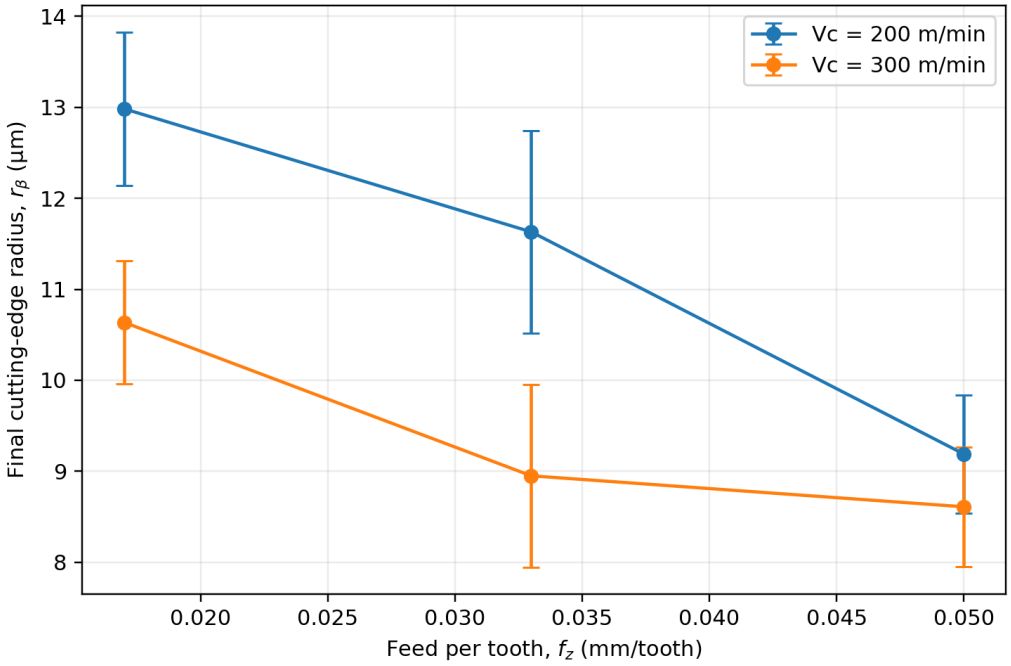


Fig. 4 Final cutting-edge radius r_β measured after machining under different combinations of cutting speed and feed per tooth.

The larger final edge radius obtained at the lowest feed per tooth may be related to the substantially greater number of tool-workpiece engagements required to machine a given cutting length when the chip load per tooth is small. Consequently, the cutting edge experiences a larger accumulated number of contacts with the highly abrasive carbon fibres. This repeated interaction may promote progressive edge rounding even when the instantaneous material removal per tooth is relatively low. The observed reduction in final edge radius at the higher cutting speed indicates, however, that the evolution of PCD edge geometry cannot be explained by a simple cutting temperature argument alone and is likely governed by the combined effects of abrasive interaction, chip load, cutting velocity and the associated wear mechanisms. A similar trend was also observed in the study by Nguyen-Dinh et al. [28], in which a PCD cutting tool with two straight cutting edges was employed.

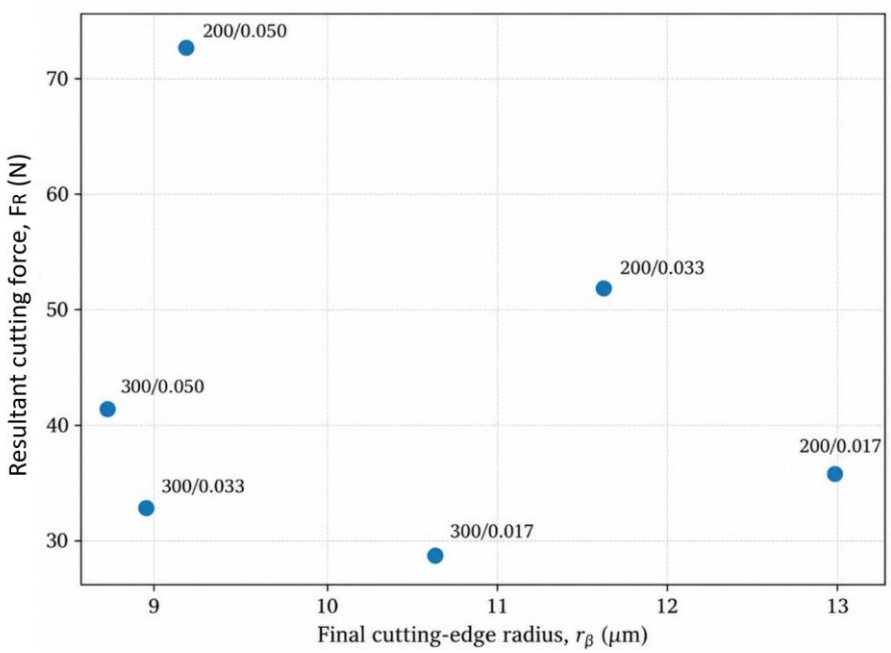


Fig. 5. Relationship between final cutting-edge radius and mean cutting force.

The relationship between edge condition and force is particularly relevant. Conditions associated with a larger final cutting edge radius generally exhibited higher cutting forces. This tendency can be visualized in Figure 5. For example, at $f_z = 0.017$mm/tooth, increasing V_c from 200 to 300 m/min reduced the final edge radius from 12.98 to 10.64 μm and simultaneously reduced the mean cutting force from 35.64 to 28.49 N. A similar tendency was found at $f_z = 0.033$mm/tooth. These observations indicate that cutting edge bluntness contributes to the resistance to CFRP removal, although the direct influence of cutting speed on cutting mechanics must also be considered. A similar trend has also been reported in the previous study by Haddad et al.[37]. The above comparison characterizes the overall relationship between final edge condition and cutting force; however, it does not capture the progressive evolution of the cutting process. This evolution was therefore examined using cumulative cutting length, L_c.

A clearer indication of progressive changes in the cutting process was obtained by expressing the measurements as a function of cumulative cutting length, L_c. The evolution of cutting force with cumulative cutting length is shown in Figure 6. The cutting force increased systematically with L_c under all six cutting conditions. The correlations between F_R and machining progression were strong, with coefficients ranging approximately from $r = 0.83$ to 0.98, and all trends were statistically significant. At $V_c = 200$m/min, the increase in force per machined face was approximately 2.79, 2.80 and 3.40 N for $f_z = 0.017, 0.033$, and 0.05 mm/tooth, respectively. At 300 m/min, the corresponding increases were approximately 2.74, 1.23 and 2.03 N per face. A similar increase in cutting force with machining distance has been reported by [11], [38], [39], who attributed this behaviour primarily to progressive tool-edge deterioration during CFRP machining. The agreement with these previous studies indicates that the force evolution observed in the present experiments follows the well-established mechanical response associated with progressive tool wear.

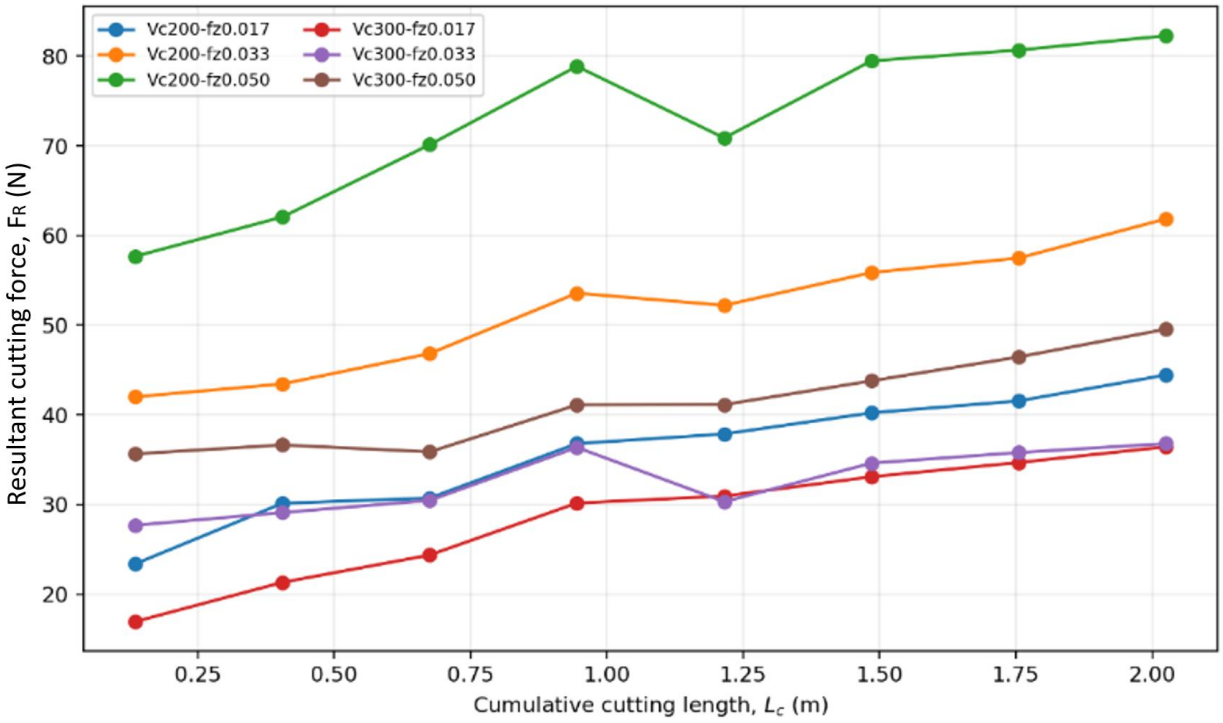


Fig. 6. Evolution of cutting force (F_R) with cumulative cutting length (L_c) under the six machining conditions.

This systematic force increase is consistent with a progressive change in cutting-edge condition during machining. Since the edge radius was measured only after completion of each cutting condition, its evolution with L_c cannot be quantified directly. Nevertheless, the combination of increasing force with accumulated cutting length and enlarged final edge radii is consistent with progressive cutting-edge rounding. Importantly, the surface-quality descriptors did not exhibit the same universal increase with L_c, indicating that the influence of cutting-edge evolution on CFRP surface integrity is substantially more complex than its effect on cutting force. These observations show that cutting force and tool-edge condition provide important information on the evolution of the cutting process, but they cannot by themselves describe the resulting surface state. The following section therefore examines how this mechanical response is reflected in the conventional profile roughness Ra and the three-dimensional areal roughness Sa.

3.2. Conventional profile roughness, R_a

The evolution of Ra as a function of machining conditions was presented in Figure 7. It is observed that the profile roughness Ra was predominantly controlled by feed per tooth. At $V_c = 200$m/min, the mean Ra increased from 0.782 μm at $f_z = 0.017$mm/tooth to 0.881 μm at $f_z = 0.033$mm/tooth and 1.527 μm at $f_z = 0.05$mm/tooth. At $V_c = 300$m/min, the corresponding values were 0.917, 0.735, and 1.426 μm. Two-way ANOVA, presented in Table 3, showed a highly significant effect of feed per tooth on Ra ($p < 10^{-8}$), accounting for approximately 84.1% of its total variation. In contrast, the effect of cutting speed was not statistically significant ($p = 0.50$), and the interaction between cutting speed and feed per tooth was also not significant at the 5% level ($p = 0.109$). These results show that Ra remains a useful descriptor of feed-related variation in CFRP surface quality. In particular, it clearly identifies the deterioration associated with the highest feed per tooth. However, its limited sensitivity to cutting speed demonstrates an important limitation. At $f_z = 0.05$mm/tooth, for example, the mean Ra values obtained at 200 and 300 m/min were very similar, 1.527and 1.426 μm, respectively. If surface quality were evaluated only using Ra, these two conditions could therefore be interpreted as producing broadly comparable surfaces.

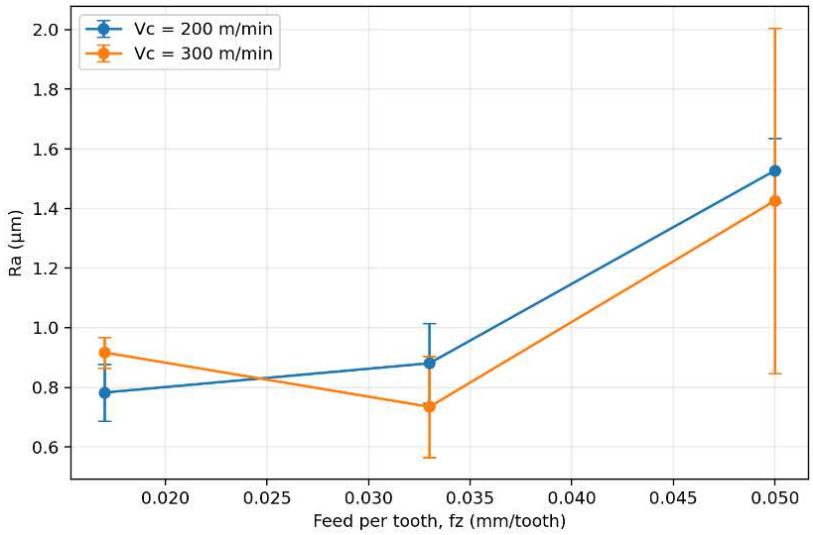


Fig. 7. Effect of cutting speed and feed per tooth on the profile roughness Ra.

The evolution of Ra with cumulative cutting length further illustrates this limitation (Figure 8). Despite the consistent increase in cutting force with L_c, Ra did not exhibit a universal increasing trend. A statistically significant increase was observed at $V_c = 200$m/min and $f_z = 0.05$mm/tooth, whereas Ra decreased significantly with cutting length at $V_c = 200$m/min, $f_z = 0.017$mm/tooth and particularly at $V_c = 300$m/min, $f_z = 0.033$mm/tooth. Under the remaining conditions, no significant systematic trend in Ra with cumulative cutting length was observed. This decoupling between cutting-force evolution and profile roughness is consistent with previous CFRP studies showing that mechanical loading, tool wear and surface quality do not necessarily evolve proportionally, because the resulting surface state is also strongly influenced by fibre orientation and local material-removal mechanisms [7], [31] .

More importantly, similar Ra values do not necessarily imply similar three-dimensional surface morphologies. This limitation is clearly illustrated by the two high-feed conditions. At $f_z = 0.05$mm/tooth, the mean Ra values at $V_c = 200$and 300 m/min were very similar, 1.527 and 1.426 µm, respectively. However, the corresponding optical images acquired using the Alicona system reveal visibly different spatial surface textures (Figure 9). The surface produced at 200 m/min exhibits a more heterogeneous appearance, with pronounced irregular bands and localized coarse surface regions, whereas the surface produced at 300 m/min appears comparatively more uniform over the analyzed region. The red rectangular boxes in Figure 9 indicate the regions of interest used for quantitative surface characterization; free-edge damage outside these regions was excluded from the analysis.

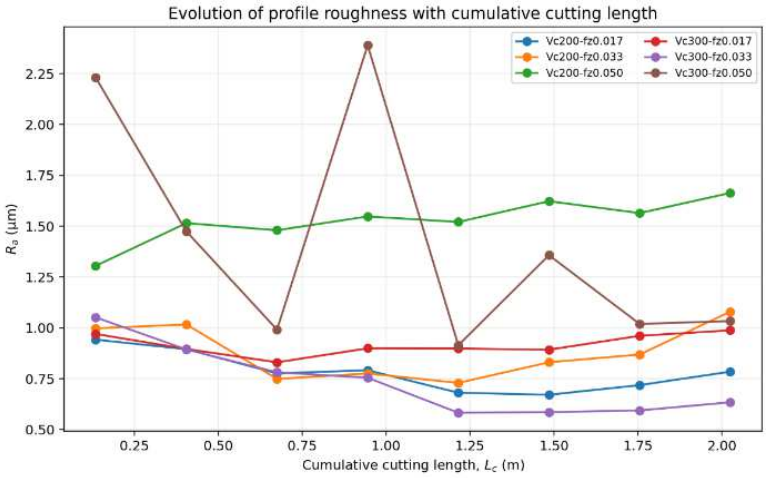


Figure 8. Evolution of profile roughness Ra with cumulative cutting length under different machining conditions.

To minimize the influence of machining progression on the visual comparison, the optical images in Figure 9 were selected from the same cumulative cutting-length position, $L_c = 0.945$m, for both cutting-speed conditions. The images are used only to illustrate spatial morphology; image intensity is not interpreted as a direct measure of surface height, so bright and dark regions are not assigned to raised or recessed features on this basis alone.

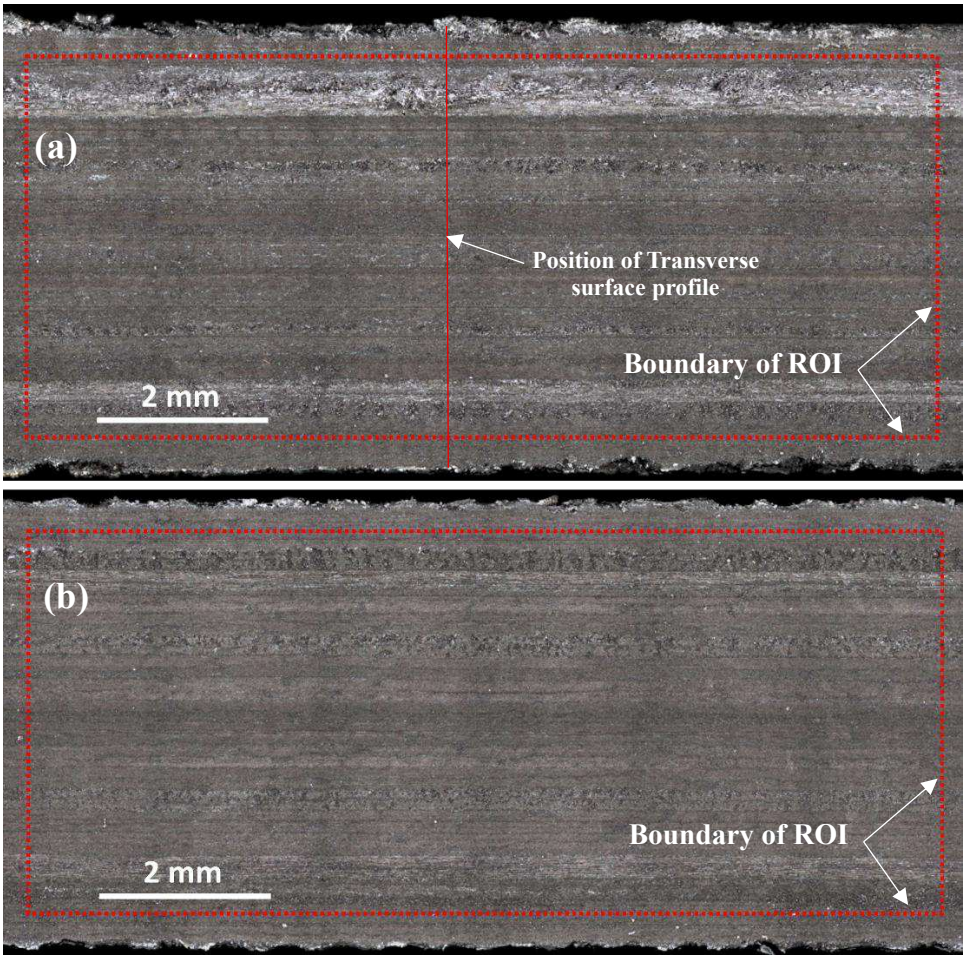


Figure 9. Optical images of surfaces machined at $f_z = 0.05$mm/tooth and $L_c = 0.945$m: (a) $V_c = 200$m/min and (b) $V_c = 300$m/min.

Additional insight into the surface morphology at $V_c = 200$m/min and $f_z = 0.05$mm/tooth is provided by the representative transverse profile shown in Figure 10. The profile contains a pronounced localized positive excursion exceeding approximately 100 µm relative to the reference level, together with smaller positive and negative deviations over the remaining measured length. This observation indicates that the high roughness response under this condition is associated with strongly localized three-dimensional surface features rather than with a uniform increase in the height of the entire surface. Because a corresponding archived transverse profile was not available for the $V_c = 300$m/min condition, Figure 10 is used only as a representative illustration of the morphology observed at 200 m/min and is not employed for direct quantitative comparison between the two cutting speeds.

Taken together, the optical observations and the representative profile demonstrate that the profile-based parameter Ra cannot fully describe the spatial heterogeneity of the machined CFRP surface. This motivates the use of the three-dimensional areal roughness Sa, which evaluates the complete measured surface rather than a single profile.

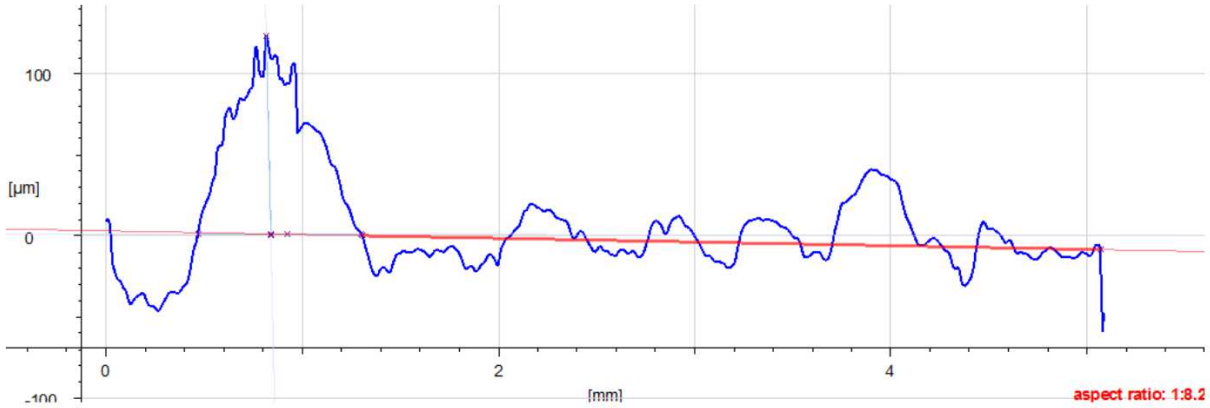


Figure 10. *Transverse surface profile for $V_c = 200$m/min and $f_z = 0.05$mm/tooth, showing a pronounced localized positive surface excursion relative to the reference level.*

3.3. Areal surface roughness, S_a

The three-dimensional areal roughness Sa exhibited a substantially stronger response to the machining parameters than Ra (Figure 11). At $V_c = 200$m/min, Sa increased from 2.52 μmat $f_z = 0.017$mm/tooth to 3.46 μmat $f_z = 0.033$mm/tooth and then increased sharply to 17.08 μmat $f_z = 0.05$mm/tooth. At $V_c = 300$m/min, the corresponding values were 2.98, 2.35, and 6.41 μm. In contrast to Ra, Sa was significantly affected by cutting speed, feed per tooth and their interaction. As summarized in Table 3, feed per tooth was the dominant factor, accounting for approximately 61.65% of the total variation in Sa. The $V_c \times f_z$ interaction contributed 21.08%, while cutting speed accounted for 12.41%. The factorial model explained 95.14% of the total variation in Sa, indicating a stronger overall sensitivity of the areal descriptor to changes in machining condition than that observed for Ra. The greater sensitivity of the areal descriptor is consistent with previous three-dimensional studies of CFRP machined surfaces, which showed that localized fibre-related defects and fibre orientation strongly affect areal topography and may not be represented adequately by a single profile-based roughness measure [24].

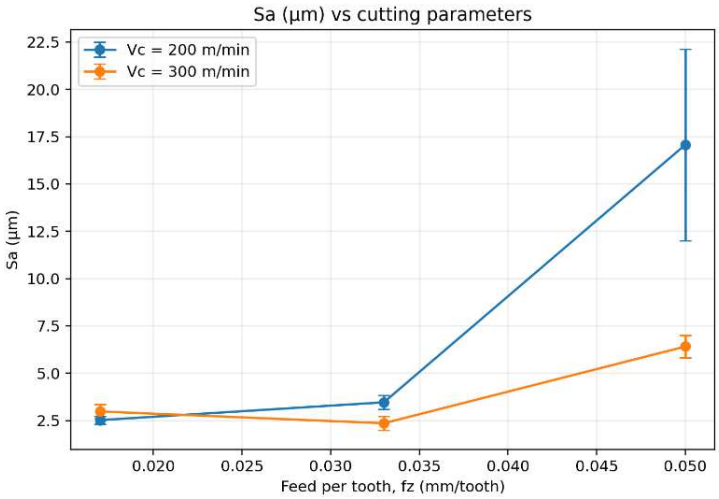


Figure 11. Effect of cutting speed and feed per tooth on the areal surface roughness Sa.

The contrast between the two high-feed conditions is particularly informative. Although Ra remained similar when the cutting speed was increased from 200 to 300 m/min at $f_z = 0.05$mm/tooth, Sa decreased markedly from 17.076 to 6.410 μm. This difference is consistent with the optical observations in Figure 9, where the surface produced at 200 m/min exhibits a more heterogeneous spatial texture than that obtained at 300 m/min. The stronger response of Sa reflects the advantage of evaluating the complete three-dimensional surface area. Machined CFRP surfaces are inherently heterogeneous, and localized topographic features may occupy only a limited fraction of the measured area. Such features can be strongly attenuated or entirely missed when surface quality is represented by a profile-based average such as Ra. In contrast, Sa incorporates the height variation over the complete analyzed surface and is therefore more sensitive to spatially localized topographic irregularity.

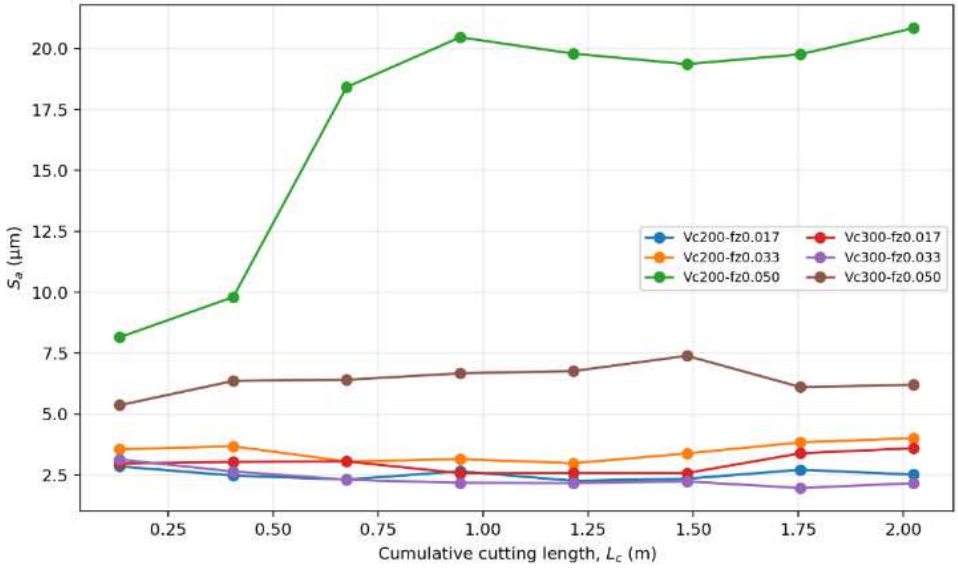


Figure 12. Evolution of areal surface roughness Sa with cumulative cutting length under different machining conditions.

The evolution of Sa with cumulative cutting length further demonstrates that the areal response is condition dependent (Figure 12). At 200 m/min and $f_z = 0.05$mm/tooth, Sa increased significantly with machining progression, consistent with the simultaneous increase in cutting force and Ra under this severe cutting condition. However, this behaviour was not universal across the six machining conditions. Under several other conditions, Sa remained approximately stable or exhibited decreasing trends despite the systematic increase in cutting force. Progressive changes in cutting

mechanics were therefore not accompanied by a consistent increase in three-dimensional roughness. However, S_a quantifies the magnitude of areal height variation without indicating whether the dominant topographic deviation lies above or below the reconstructed reference surface.

3.4. Above-surface volume

The separated volumetric descriptors were therefore examined to resolve the positive and negative contributions relative to the reconstructed ISO-surface. The Above Surface Volume exhibited the strongest interaction between cutting speed and feed per tooth among the investigated surface descriptors (Figure 13). At $V_c = 200$m/min, the mean above-surface volume increased moderately from 0.122 mm^{3}at $f_z = 0.017$mm/tooth to 0.150 mm^{3}at $f_z = 0.033$mm/tooth, before increasing sharply to 0.975 mm^{3}at $f_z = 0.05$mm/tooth. In contrast, at $V_c = 300$m/min the corresponding values were 0.107, 0.034, and 0.106 mm^3. Therefore, increasing the feed to 0.05 mm/tooth generated a large above-surface volumetric response at 200 m/min but not at 300 m/min. As summarized in Table 3, ANOVA confirmed highly significant effects of cutting speed, feed per tooth and their interaction on Above Surface Volume, with all p-values below 10^{-8}. The feed effect accounted for approximately 38.21% of the total variation, the interaction for 32.53%, and cutting speed for 24.84%. The large interaction contribution indicates that the effect of feed on the above-surface volumetric response depends strongly on cutting speed.

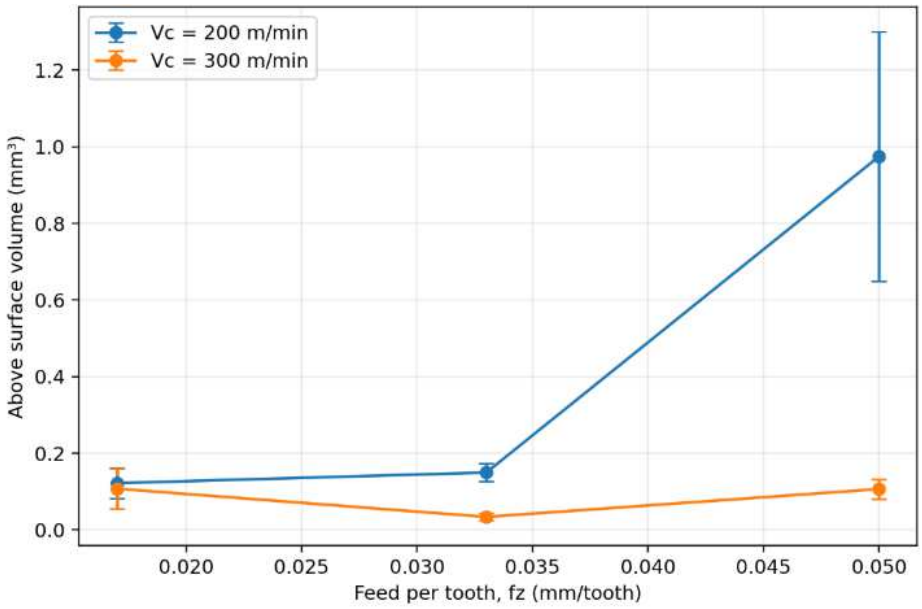


Figure 13. Effect of cutting speed and feed per tooth on Above Surface Volume measured using the Alicona Volume Measurement method.

The condition $V_c = 200$m/min and $f_z = 0.05$mm/tooth is particularly noteworthy because it simultaneously exhibited the highest $Sa$and by far the largest Above Surface Volume in the dataset. Its mean Sa was 17.076 µm and its Above Surface Volume reached 0.975 mm³, compared with 6.410 µm and 0.106 mm³, respectively, at $V_c = 300$m/min under the same feed per tooth. This result indicates that the exceptionally large areal roughness at 200 m/min was predominantly associated with topographic volume located above the reconstructed ISO-surface.

This distinction could not be inferred from Ra. At the same two high-feed conditions, Ra changed only from 1.527 to 1.426 µm as cutting speed increased from 200 to 300 m/min. Thus, a relatively small change in the profile roughness accompanied an approximately nine-fold reduction in Above Surface Volume. This comparison demonstrates that the volumetric descriptor is substantially more sensitive to changes in the three-dimensional distribution of the surface topography than Ra.

The evolution of Above Surface Volume with cumulative cutting length was also strongly condition dependent (Figure 14). At $V_c = 200$m/min and $f_z = 0.05$mm/tooth, Above Surface Volume showed a positive trend with machining progression, consistent with the simultaneous increases in F_t, Ra and Sa, although the linear trend in Above Surface Volume itself did not reach the 5% significance level. In contrast, at $V_c = 300$m/min and $f_z = 0.017$mm/tooth, Above

Surface Volume increased significantly with cumulative cutting length even though neither Ra nor Sa exhibited a significant monotonic increase. These results show that machining progression can alter the balance of three-dimensional topographic features without producing a corresponding monotonic change in conventional roughness parameters. The Above Surface Volume therefore provides information on the evolution of positive topographic deviation that is not captured consistently by either Ra or Sa.

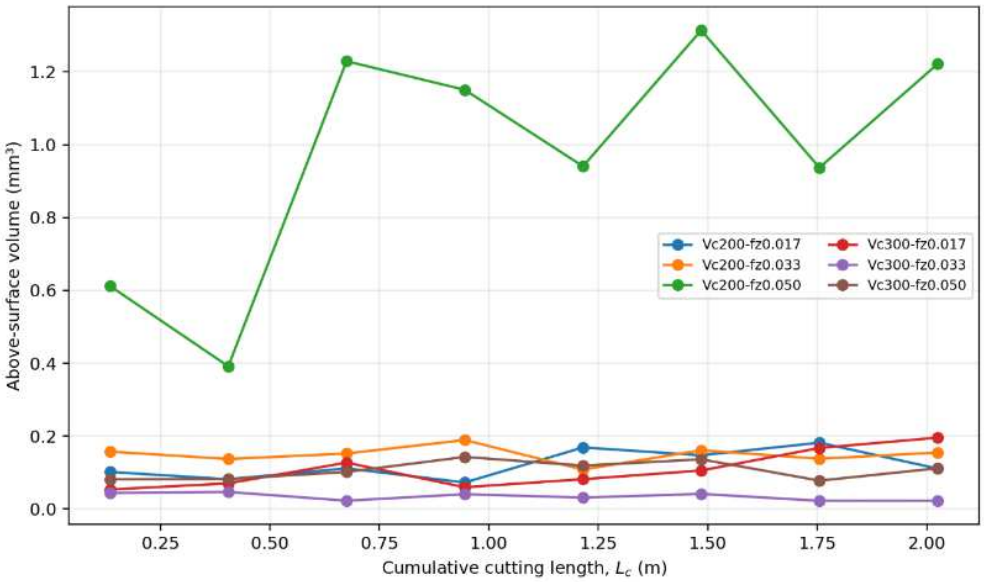


Figure 14. Evolution of Above Surface Volume with cumulative cutting length under the six machining conditions.

While the Above Surface Volume characterizes the positive volumetric deviation from the reconstructed ISO-surface, a complete description of the surface topography also requires consideration of the corresponding negative deviation. The Below Surface Volume was therefore examined separately to determine whether the machining parameters produced a similar or fundamentally different response below the reference surface.

3.5. Below-surface volume

The Below Surface Volume showed an entirely different response from the Above Surface Volume as presented in Figure 15. At $V_c = 200$m/min, the mean below-surface volume remained comparatively small, increasing only from 0.019 mm^{3}at $f_z = 0.017$mm/tooth to 0.029 mm^{3}at $f_z = 0.033$mm/tooth and 0.033 mm^{3}at $f_z = 0.05$mm/tooth. At $V_c = 300$m/min, however, the Below Surface Volume increased strongly with feed, from 0.040 mm^{3}at $f_z = 0.017$mm/tooth to 0.093 mm^{3}at $f_z = 0.033$mm/tooth and 0.231 mm^{3}at $f_z = 0.05$mm/tooth.

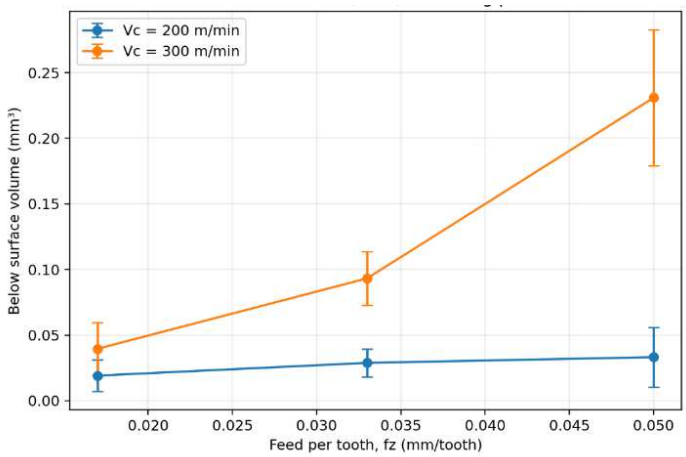


Figure 15. Effect of cutting speed and feed per tooth on Below Surface Volume measured using the Alicona Volume Measurement method.

The results in Table 3 show that cutting speed, feed per tooth and their interaction all had statistically significant effects on Below Surface Volume. Cutting speed accounted for approximately 38.26% of the total variation, feed per tooth for 31.81%, and the interaction ($V_c \times f_z$) for 24.5%. The factorial model explained 94.58% of the total variation. These results indicate that the development of negative topographic volume relative to the reconstructed ISO-surface depends on the combined cutting condition rather than on feed per tooth alone.

The comparison between the two high-feed conditions provides the clearest evidence of this behaviour. At $f_z = 0.05$mm/tooth and $V_c = 200$m/min, the volumetric response was strongly above-surface dominated, with $V_{\text{above}} = 0.975$mm³ and $V_{\text{below}} = 0.033$mm³. In contrast, at $V_c = 300$m/min, V_{above} decreased to 0.106 mm³ while V_{below}increased to 0.231 mm³. Increasing cutting speed therefore produced a clear inversion in the dominant volumetric response, from predominantly positive to predominantly negative topographic deviation relative to the reconstructed ISO-surface.

This inversion is largely obscured when the same surfaces are characterized using Ra. Their mean Ra values were 1.527 and 1.426 µm, respectively, differing by only approximately 0.10 µm. Sa was considerably more sensitive, decreasing from 17.076 to 6.410 µm, and therefore clearly identified a substantial change in the overall magnitude of three-dimensional surface irregularity. However, Sa alone cannot indicate whether this irregularity is dominated by topographic volume above or below the reference surface.

The separated Above and Below Surface Volumes therefore provide complementary information that cannot be obtained from either Ra or Sa alone. Ra describes profile-scale roughness and Sa quantifies the overall magnitude of three-dimensional surface irregularity, whereas the volumetric descriptors additionally distinguish the direction of the dominant topographic deviation relative to the reconstructed reference surface. Whereas previous volumetric characterization of CFRP machining has focused primarily on crater-volume measures used alongside S_a and X-ray tomography [28], the present approach separates the volumetric response into above- and below-surface components, enabling the direction of the dominant topographic deviation to be distinguished explicitly.

The evolution of Below Surface Volume with cumulative cutting length further emphasizes that machining progression does not produce a universal change in surface morphology (Figure 16). In particular, at $V_c = 300$m/min and $f_z = 0.017$mm/tooth, Below Surface Volume decreased significantly with increasing L_c, while Above Surface Volume increased significantly. At the same time, cutting force increased strongly, whereas neither Ra nor Sa exhibited a significant monotonic trend. This opposite evolution of the two volumetric components demonstrates that machining progression can change the relative balance between positive and negative topographic deviations without producing a corresponding monotonic response in conventional roughness parameters.

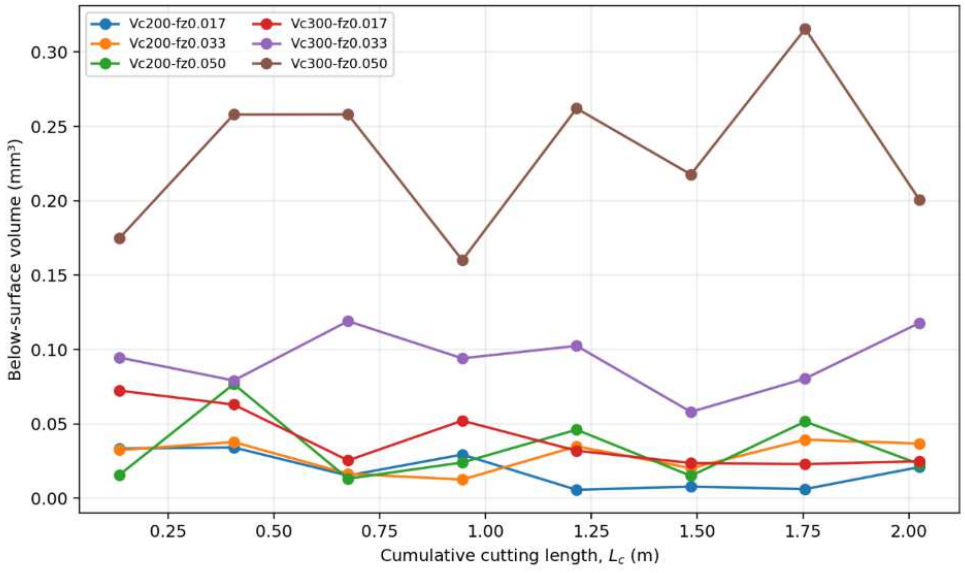


Fig. 16. Evolution of Below Surface Volume with cumulative cutting length under different machining conditions.

To provide independent qualitative evidence for the below-surface response, µCT observations were obtained for the two high-feed conditions, $V_c = 200$ and 300 m/min at $f_z = 0.05$mm/tooth, at the same depth of 100 µm below the machined surface (Figure 17). Moreover, for consistency with the optical comparison, the µCT observations were obtained from the same cumulative cutting-length position, $L_c = 0.945$m, for both high-feed conditions. A clear difference was observed between the two conditions. The specimen machined at 300 m/min exhibited more numerous and more extensive localized low-density/discontinuous regions, whereas the corresponding specimen machined at 200 m/min appeared comparatively more uniform. This qualitative difference is consistent with the Alicona volumetric measurements. At 300 m/min, the substantially larger Below Surface Volume ($0.231\ \mathrm{mm}^3$) was accompanied by a greater occurrence of µCT-visible discontinuities, whereas the 200 m/min condition exhibited a much smaller Below Surface Volume ($0.033\ \mathrm{mm}^3$) and fewer such features. The µCT observations therefore provide independent qualitative support for the physical relevance of the separated below-surface volumetric response. The presence of condition-dependent subsurface discontinuities is consistent with previous investigations showing that subsurface damage in CFRP milling is strongly influenced by cutting parameters, fibre cutting angle and cutting-edge geometry [32] . Because the present µCT comparison is qualitative, the observed regions are not assigned to a specific fibre- or matrix-scale damage mechanism without further segmentation or three-dimensional defect analysis.

.

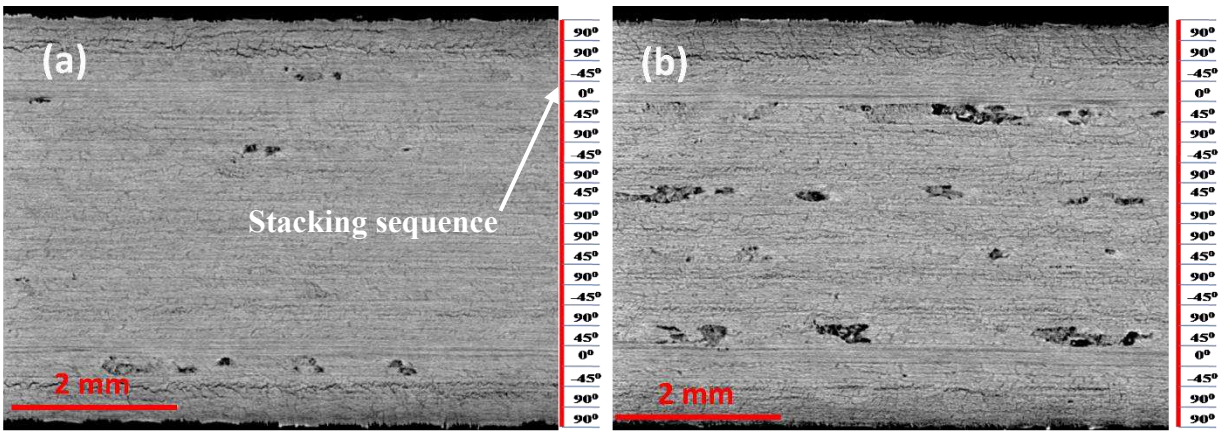


Figure 17. Reconstructed µCT images at a depth of 100 µm below the machined surface for $f_z = 0.05$mm/tooth and $L_c = 0.945$m: (a) $V_c = 200$m/min and (b) $V_c = 300$m/min.

The agreement between the volumetric and µCT observations suggests that the high-feed inversion reflects a change in the form of material removal rather than merely a change in roughness magnitude. Because f_z remained fixed at 0.05 mm/tooth, the inversion cannot be attributed to a change in nominal chip load. Instead, increasing cutting speed changes the rate and dynamics of tool–material interaction and may modify the balance between fibre bending, incomplete separation, localized fracture and material-removal events across the different fibre orientations of the multidirectional laminate. Under this interpretation, the strongly positive volumetric response at 200 m/min is consistent with a greater contribution from localized features remaining above the reconstructed reference surface, whereas the larger negative volume at 300 m/min is consistent with a greater contribution from removal events leaving subsurface or material-deficit-type discontinuities. The µCT observations support the existence of physically different surface/subsurface states, although the specific fibre- and matrix-scale mechanisms cannot be identified from the present data alone.

Because the Above and Below Surface Volumes are extensive quantities, their absolute values may in principle depend on the size of the analyzed surface region. To verify that the volumetric differences identified above were not caused by small variations in the projected ROI area, the volumetric response was additionally normalized by the projected area, A_p.

$$V_{\mathrm{above,n}} = \frac{V_{\mathrm{above}}}{A_p},\ V_{\mathrm{below,n}} = \frac{V_{\mathrm{below}}}{A_p}. \tag{2}$$

The total normalized volumetric deviation was additionally calculated as Eq. (3):

$$V_{\mathrm{tot,n}} = \frac{V_{\mathrm{above}} + V_{\mathrm{below}}}{A_p}. \quad (3)$$

where A_p is the projected area of the analyzed region. Since the volumes are expressed in mm³ and A_p in mm², multiplication by 1000 expresses the normalized quantity in micrometres. $V_{\mathrm{total,n}}$ therefore represents an equivalent mean total volumetric deviation per unit projected area, combining the contributions above and below the reconstructed ISO-surface. The projected area was highly consistent among the experimental conditions, with condition means ranging only from approximately 44.45 to 44.84 mm². Consequently, the large differences observed in Above and Below Surface Volume cannot be attributed to substantial variations in the analyzed surface area. From the results in Figure 18, it is observed that at $V_c = 200$m/min, the normalized total volumetric deviation increased from approximately 3.15 µm at $f_z = 0.017$mm/tooth to 4.00 µm at $f_z = 0.033$mm/tooth, before increasing sharply to 22.66 µm at $f_z = 0.05$mm/tooth. At $V_c = 300$m/min, the corresponding values were 3.28, 2.84 and 7.59 µm. Thus, the normalized response reproduced the same strong high-feed contrast identified using the raw volumetric quantities. The pronounced peak at 200 m/min and 0.05 mm/tooth was dominated by the Above Surface Volume because its magnitude (0.975 mm³) greatly exceeded the corresponding Below Surface Volume (0.033 mm³), whereas the relative contribution of the below-surface component was greater at 300 m/min under the same feed condition.

The statistical response of the normalized descriptor was consistent with that of the raw volumetric quantities: feed per tooth remained the dominant factor, while cutting speed and the $V_c \times f_z$ interaction also exerted statistically significant effects. Importantly, normalization did not alter the principal trends or the relative ranking of the machining conditions. The close agreement between the raw and normalized results confirms that the large volumetric differences observed in this study cannot be attributed to small variations in ROI size. Rather, they reflect genuine differences in the measured three-dimensional surface topography. The raw Above and Below Surface Volumes were therefore retained as the principal engineering responses, whereas $V_{\mathrm{total,norm}}$ was used as an area-normalized robustness descriptor.

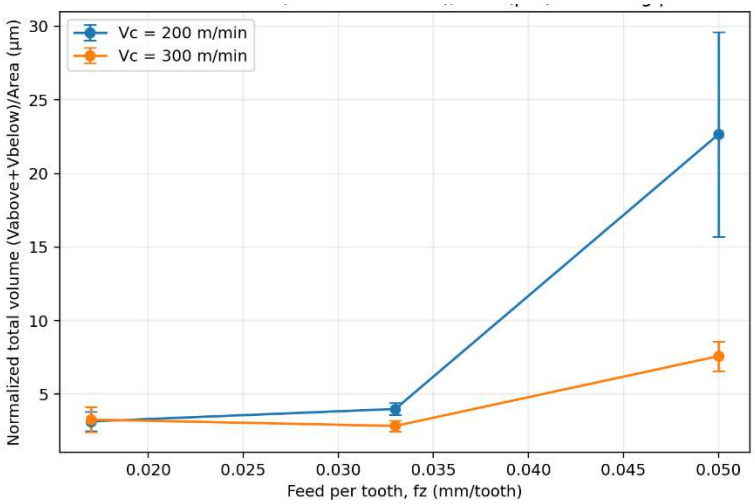


Figure 18. Effect of cutting speed and feed per tooth on the normalized total volumetric deviation, $V_{\mathrm{total,n}}$.

3.6. Relationships among surface descriptors and cutting mechanics

Having established that the volumetric trends remained unchanged after normalization by projected area, the relationships among Ra, Sa, and the volumetric descriptors were examined to determine whether these parameters contain redundant or complementary information. Their relationships with cutting force were also evaluated to assess whether the mechanical loading of the cutting process could be used as a direct indicator of the resulting surface condition.

Across the 48 machined surfaces, R_a and S_a exhibited only a moderate positive correlation (r = 0.659; Figure 19), indicating only partial overlap between profile and areal roughness. S_a correlated strongly with Above Surface Volume (r = 0.950) and with the normalized total volumetric deviation, whereas its relationship with Below Surface Volume was weak (r = -0.027; Figure 20). The weak S_a-Below Surface Volume association is particularly important because it shows that the below-surface component varied largely independently of the overall areal roughness magnitude.

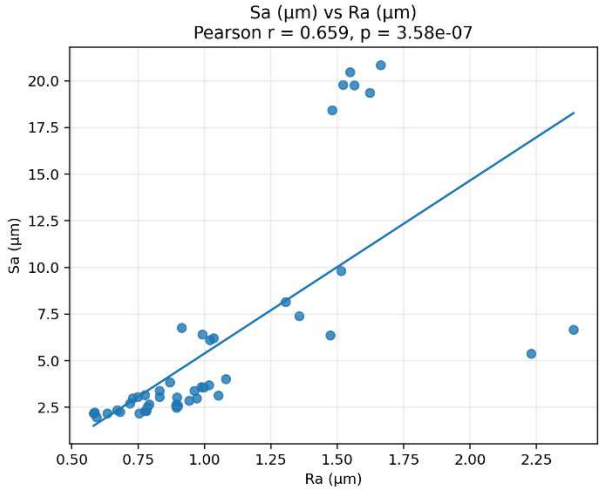


Figure 19. Relationship between profile roughness Ra and areal roughness Sa for the 48 machined surfaces.

This distinction is particularly evident for the high-feed conditions discussed in Sections 3.3–3.5. At $V_c = 300$m/min and $f_z = 0.05$mm/tooth, the surface exhibited a substantial Below Surface Volume despite a considerably lower Sa than the corresponding 200 m/min condition. Therefore, Sa is more sensitive than Ra to three-dimensional surface variation, but it cannot distinguish whether that variation is dominated by positive or negative volumetric deviation relative to the reconstructed reference surface.

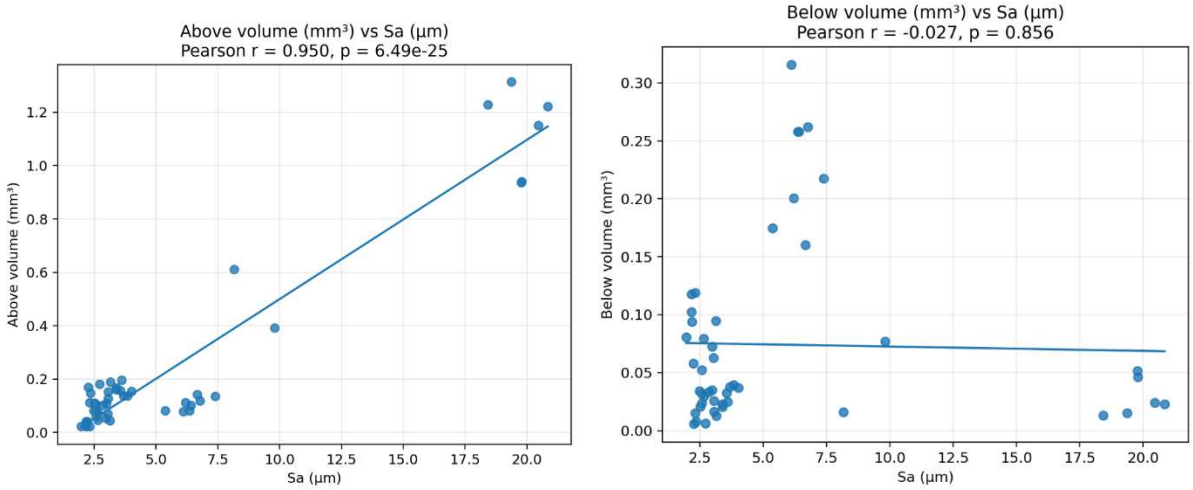


Figure 20. Relationship between (a) Sa and Above Surface Volume and (b) Sa and Below Surface Volume.

Because pooled correlations can partly arise from the simultaneous influence of cutting speed and feed per tooth on several responses, within-condition correlations were also evaluated after subtracting the corresponding cutting-condition means. Under this analysis, the relationship between Ra and normalized total volumetric deviation became negligible, whereas the relationship between Sa and normalized total volumetric deviation remained strong. Similarly, the within-condition association between Sa and Above Surface Volume remained appreciable. These results provide additional evidence that areal roughness is more closely associated with three-dimensional volumetric topography than profile roughness, even after the common influence of the machining parameters is reduced.

The relationship between cutting force and the surface descriptors provides a complementary mechanical perspective as exhibited in Figure 21. Across the complete dataset, cutting force showed a moderate correlation with Ra ($r = 0.475$), but substantially stronger correlations with Sa ($r = 0.836$) and Above Surface Volume ($r = 0.842$). In contrast, the correlation between cutting force and Below Surface Volume was weak and slightly negative ($r =$

-0.175). After removing the cutting-condition means, the force–Ra relationship became negligible, whereas moderate relationships remained between cutting force and both $Sa$and Above Surface Volume.

These results demonstrate that increasing mechanical cutting load does not correspond to a uniform increase in every form of surface irregularity. This is particularly evident at $f_z = 0.05$mm/tooth, where increasing cutting speed from 200 to 300 m/min reduced the mean cutting force from approximately 72.75 to 41.27 N, while Below Surface Volume increased markedly from 0.033 to 0.231 mm³. Therefore, a lower cutting force cannot automatically be interpreted as improved surface condition, because changes in machining conditions may reduce the mechanical load while simultaneously altering the dominant topographic response of the machined surface.

Taken together, the correlation and cumulative-length analyses show that the investigated descriptors are complementary rather than interchangeable. Ra remains useful for detecting feed-related changes in profile roughness, whereas Sa provides greater sensitivity to three-dimensional surface variation. The separated Above and Below Surface Volumes extend this characterization by retaining information on the direction of the volumetric deviation relative to the reconstructed reference surface. At the same time, the progressive increase in cutting force with cumulative cutting length did not produce a universal increase in any single surface descriptor. The value of the volumetric approach therefore lies not in replacing conventional roughness parameters, but in revealing three-dimensional topographic information that Ra, Sa, or cutting force alone cannot provide.

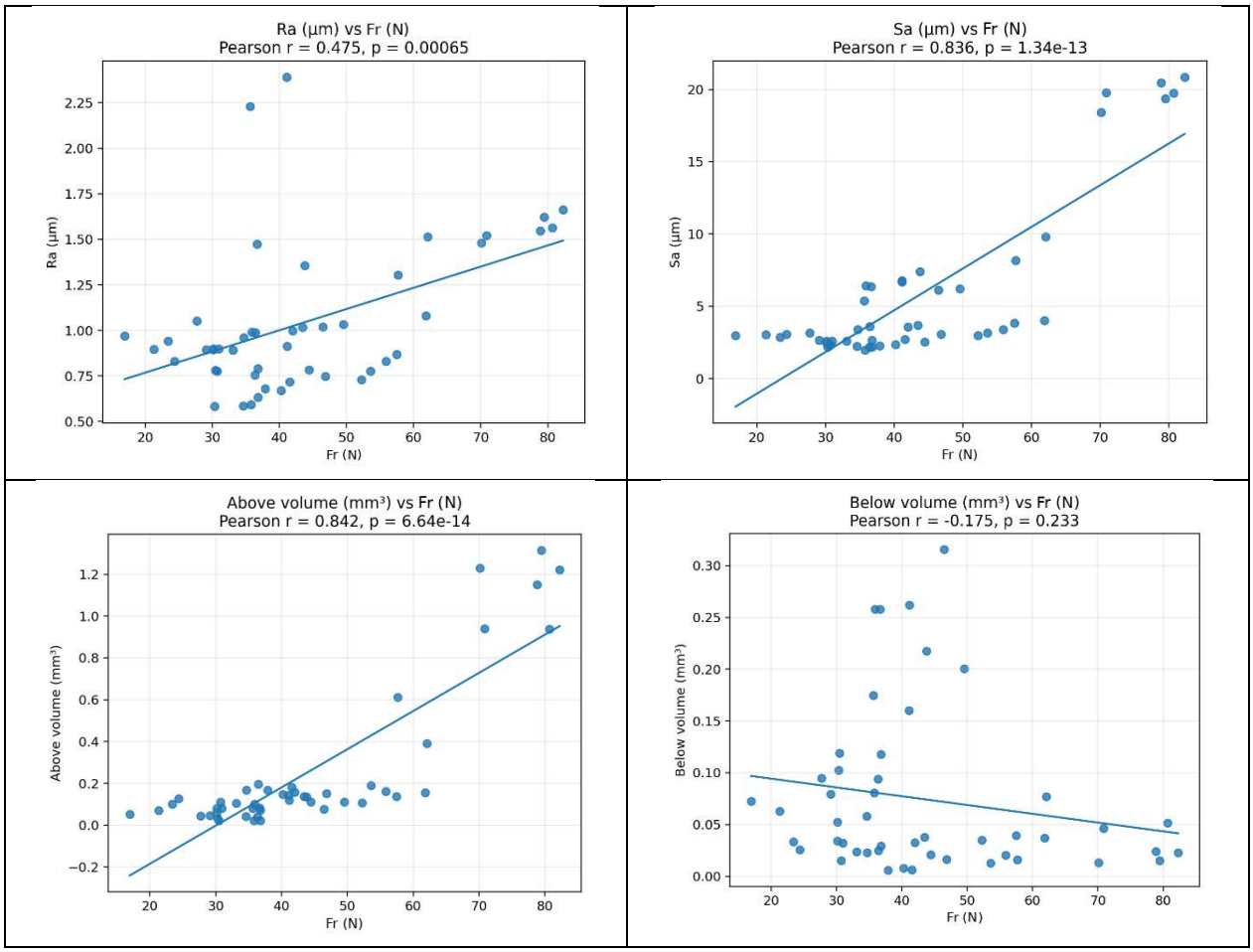


Figure 21. Relationships between cutting force and surface-quality descriptors: (a) Ra, (b) Sa, (c) Above Surface Volume, and (d) Below Surface Volume.

Several limitations of the present study should be acknowledged. The surface measurements were performed over a nominal ROI of approximately 45 mm² located within the machined surface, with free-edge damage intentionally excluded; therefore, the reported descriptors characterize the local machined-surface state rather than the complete

specimen surface. The factorial analysis was based on four independent specimens per machining condition, while the two faces of each specimen were treated as paired measurements. The μCT observations were limited to a qualitative comparison of the two high-feed conditions at a common depth of 100 μm and were not subjected to three-dimensional segmentation or quantitative defect analysis. In addition, the present work focused on surface topography and machining mechanics and did not directly establish relationships between the proposed volumetric descriptors and the post-machining mechanical properties of the machined CFRP specimens. These aspects provide important directions for further validation of the volumetric characterization approach.

4. Conclusions

This study compared conventional profile roughness, three-dimensional areal roughness and separated volumetric descriptors for characterizing milled CFRP surfaces under different cutting speeds, feed per tooth values and cumulative cutting lengths. The following conclusions can be drawn:

1. Cutting mechanics were strongly dependent on the machining condition. Cutting force increased with feed per tooth and decreased when cutting speed was increased from 200 to 300 m/min. Cutting force also increased systematically with cumulative cutting length, while the final cutting-edge measurements were consistent with progressive changes in tool condition during machining.
2. Ra remained useful for identifying feed-related roughness changes but showed limited sensitivity to cutting speed. Feed per tooth accounted for 84.1% of the total variation in Ra, whereas cutting speed and the $V_c \times f_z$ interaction were not statistically significant. In contrast, Sa was significantly affected by cutting speed, feed per tooth and their interaction, demonstrating greater sensitivity to three-dimensional changes in the machined surface.
3. The separated Above and Below Surface Volumes revealed information that could not be obtained from either Ra or Sa alone. At $f_z = 0.05$mm/tooth, increasing cutting speed from 200 to 300 m/min changed Ra only from 1.527 to 1.426 μm, whereas the volumetric response changed from strongly above-surface dominated V_{above} = 0.975 mm^3, V_{below} = 0.033 mm^3 to below-surface dominated (V_{above} = 0.106 mm^3, V_{below} = 0.231 mm^3). This demonstrates that comparable profile roughness does not necessarily correspond to comparable three-dimensional surface states.
4. The physical relevance and robustness of the volumetric response were supported by independent analyses. Qualitative μCT observations at a common depth of 100 μm showed more numerous and extensive localized discontinuities for the 300 m/min high-feed condition, consistent with its substantially larger Below Surface Volume. In addition, normalization by projected area reproduced the same principal volumetric trends, confirming that the observed differences were not caused by small variations in ROI size.
5. Machining progression and cutting force did not produce a universal change in surface quality. Although cutting force increased consistently with cumulative cutting length, Ra, Sa, $V_{\mathrm{above}}$and V_{below} evolved differently depending on the machining condition. Correlation analysis similarly showed that neither cutting force nor a single roughness parameter can fully represent the resulting CFRP surface state.
6. The investigated descriptors are therefore complementary rather than interchangeable. Ra describes profile-scale roughness, Sa captures the magnitude of three-dimensional areal variation, while V_{above} and V_{below} additionally retain information on the direction and volumetric extent of the topographic deviation relative to the reconstructed reference surface. Volumetric characterization should therefore be used as a complement to, rather than a replacement for, conventional roughness measurements when a more complete description of machined CFRP surfaces is required.

Overall, the results demonstrate that machined CFRP surface quality cannot be represented adequately by a single roughness parameter when the objective is to distinguish different three-dimensional surface states. The combined use of profile, areal and separated volumetric descriptors provides a more physically informative basis for relating machining conditions and cutting mechanics to the resulting surface topography.

5. References

[1] Arola D, Ramulu M (1994) Machining-induced surface texture effects on the flexural properties of a graphite/epoxy laminate. Composites 25(8):822–834. https://doi.org/10.1016/0010-4361(94)90143-0

[2] Arola D, Ramulu M (1997) Net shape manufacturing and the performance of polymer composites under dynamic loads. Experimental Mechanics 37(4):379–385. https://doi.org/10.1007/BF02317300

[3] Arola D, Ramulu M (1999) An examination of the effects from surface texture on the strength of fiber reinforced plastics. Journal of Composite Materials 33(2):102–123. https://doi.org/10.1177/002199839903300201

[4] Duboust N, Watson M, Marshall M, O'Donnel GE, Kerrigan K (2021) Towards intelligent CFRP composite machining: surface analysis methods and statistical data analysis of machined fibre laminate surfaces. Proceedings of the Institution of Mechanical Engineers, Part B: Journal of Engineering Manufacture 235(10):1602–1617. https://doi.org/10.1177/0954405420960920

[5] Zhang L, Zhang X (2023) Effect of cooling and lubrication conditions on the variable angle milling of unidirectional CFRP with PCD tools. Journal of Materials Processing Technology 319:118073. https://doi.org/10.1016/j.jmatprotec.2023.118073

[6] Bukor L, Fu R, Geier N (2026) Influence of top-surface condition and process parameters on cutting forces and surface integrity in CFRP milling. The International Journal of Advanced Manufacturing Technology 145:8907–8924. https://doi.org/10.1007/s00170-026-18809-9

[7] Son J, Mungale C, Baruah S, Vaidya U, Schmitz T (2025) Tool wear, mechanistic force modeling, and surface finish in CFRP milling. Journal of Manufacturing Processes 141:1397–1415. https://doi.org/10.1016/j.jmapro.2025.03.068

[8] Wu W et al (2024) Tool wear influence on surface roughness, burrs and cracks in milling unidirectional carbon fiber reinforced plastics (UD-CFRP). Journal of Materials Research and Technology 30:3052–3065. https://doi.org/10.1016/j.jmrt.2024.04.064

[9] Slamani M, Chatelain JF (2023) A review on the machining of polymer composites reinforced with carbon (CFRP), glass (GFRP), and natural fibers (NFRP). Discover Mechanical Engineering 2:4. https://doi.org/10.1007/s44245-023-00011-w

[10] Cepero-Mejias F, Duboust N, Phadnis VA, Kerrigan K, Curiel-Sosa JL (2021) A novel finite element method approach in the modelling of edge trimming of CFRP laminates. Applied Sciences 11(11):4743. https://doi.org/10.3390/app11114743

[11] Qiu J, Zhang S, Li B, Li Y, Wang L (2023) Research on tool wear and surface integrity of CFRPs with mild milling parameters. Coatings 13(1):207. https://doi.org/10.3390/coatings13010207

[12] Thi-Hue N, Dinh-Ngoc N (2023) Influences of main machining process parameters and tool wear on the machining damage generated during edge milling CFRP composites. Journal of Mechanical Engineering 20(3):355–370. https://doi.org/10.24191/jmeche.v20i3.23917

[13] Xu Z, Wang Y (2022) Study on milling force and surface quality during slot milling of plain-woven CFRP with PCD tools. Materials 15(11):3862. https://doi.org/10.3390/ma15113862

[14] Wang C, Wen L, Ming W, An Q, Chen M (2018) Experimental study on effects of fiber cutting angle in milling of high-strength unidirectional carbon fiber-reinforced polymer laminates. Proceedings of the Institution of Mechanical Engineers, Part B: Journal of Engineering Manufacture 232(10):1813–1824. https://doi.org/10.1177/0954405416679868

[15] Mustafa AM, Shahruddin NS, Abd Halim NFH, Rozhan AN, Hattiar MA (2022) The effect of cutting speeds on tool wear and surface roughness when milling carbon fiber reinforced polymer. IOP Conference Series: Materials Science and Engineering 1244(1):012018. https://doi.org/10.1088/1757-899X/1244/1/012018

[16] Zhang L, Zhang X (2023) A comparative experimental study of unidirectional CFRP high-speed milling in up and down milling with varied angles. Journal of Manufacturing Processes 101:1147–1157. https://doi.org/10.1016/j.jmapro.2023.06.064

[17] Kim DG, Yang SH (2024) Uncut fiber analysis using fiber deflection and cutting forces in carbon fiber-reinforced plastics during rotation of the cutting tool. Composites Part A: Applied Science and Manufacturing 182:108206. https://doi.org/10.1016/j.compositesa.2024.108206

[18] Mustafa AM, Abd Halim NFH, Dahnel AN, Ali A, Ahmad Z (2025) Milling-induced surface roughness in carbon fiber reinforced polymer: a diagnostic study between Ra and Sa. Mekatronika: Journal of Intelligent Manufacturing and Mechatronics 7(2):142–148. https://doi.org/10.15282/mekatronika.v7i2.12957

[19] Böhland F, Tutunea Fatan R, Schulze V (2025) Formation and occurrence of subsurface damage mechanism with the analysis of optimal machining strategy when milling different fibre matrix combination of unidirectional FRP's. Journal of Thermoplastic Composite Materials 38(8):2995–3019. https://doi.org/10.1177/08927057251331573

[20] Squires CA, Netting KH, Chambers AR (2007) Understanding the factors affecting the compressive testing of unidirectional carbon fibre composites. Composites Part B: Engineering 38(4):481–487. https://doi.org/10.1016/j.compositesb.2006.08.002

[21] Ghidossi P, El Mansori M, Pierron F (2004) Edge machining effects on the failure of polymer matrix composite coupons. Composites Part A: Applied Science and Manufacturing 35(7–8):989–999. https://doi.org/10.1016/j.compositesa.2004.01.015

[22] Haddad M, Zitoune R, Bougherara H, Eyma F, Castanié B (2014) Study of trimming damages of CFRP structures in function of the machining processes and their impact on the mechanical behavior. Composites Part B: Engineering 57:136–143. https://doi.org/10.1016/j.compositesb.2013.09.051

[23] Cai C, Dang J, An Q, Ming W, Chen M (2022) Surface morphology characterization of unidirectional carbon fibre reinforced plastic machined by peripheral milling. Chinese Journal of Aeronautics 35(2):361–375. https://doi.org/10.1016/j.cja.2021.04.024

[24] An Q et al (2025) Fiber orientation effects in CFRP milling: multiscale characterization of cutting dynamics, surface integrity, and damage mechanisms. Journal of Composites Science 9(7):342. https://doi.org/10.3390/jcs9070342

[25] Wang F, Bi G, Wang X, Zhao X (2021) Influences of milling strategies and process parameters on the cavity defect generated during milling of carbon fiber reinforced polymer. Proceedings of the Institution of Mechanical Engineers, Part C: Journal of Mechanical Engineering Science 235(4):723–733. https://doi.org/10.1177/0954406220938399

[26] Sourd X, Zitoune R, Crouzeix L, Coulaud M, Lamouche D (2021) Influence of the damage generated by abrasive water jet texturing on the tensile static and fatigue behaviour of 3D woven composite in the context of repair. Composites Part A: Applied Science and Manufacturing 149:106567. https://doi.org/10.1016/j.compositesa.2021.106567

[27] Nguyen-Dinh N, Bouvet C, Zitoune R (2020) Influence of machining damage generated during trimming of CFRP composite on the compressive strength. Journal of Composite Materials 54(11):1413–1430. https://doi.org/10.1177/0021998319883335

[28] Nguyen-Dinh N, Zitoune R, Bouvet C, Leroux S (2019) Surface integrity while trimming of composite structures: X-ray tomography analysis. Composite Structures 210:735–746. https://doi.org/10.1016/j.compstruct.2018.12.006

[29] Li J, Xu K, Lin Z, Fu J (2024) A unified geometrical modeling and analysis method for evaluating CFRP machining performance: cutting geometry space. Composites Part B: Engineering 283:111649. https://doi.org/10.1016/j.compositesb.2024.111649

[30] Sourd X, Zitoune R, Hejjaji A, Salem M, Crouzeix L, Lamouche D (2020) Multi-scale analysis of the generated damage when machining pockets of 3D woven composite for repair applications using abrasive water jet process: contamination analysis. Composites Part A: Applied Science and Manufacturing 139:106118. https://doi.org/10.1016/j.compositesa.2020.106118

[31] He Y, Fan Y, Wang D, Zitoune R, Luo J, Qi J (2025) The cutting performance of coated and uncoated segmented flute routers with tool wear progression in milling multidirectional CFRP composites. Wear 578–579:206199. https://doi.org/10.1016/j.wear.2025.206199

[32] Böhland F, Hilligardt A, Schulze V (2024) Analysis of subsurface damage during milling of CFRP due to spatial fibre cutting angle, tool geometry and cutting parameters. Composites Part B: Engineering 281:111533. https://doi.org/10.1016/j.compositesb.2024.111533

[33] Dang AT, Nguyen DN (2026) Analysis of the machinability of multidirectional CFRP laminates. Journal of Materials Engineering and Performance 35(13):12852–12869. https://doi.org/10.1007/s11665-025-12491-w

[34] Alicona Imaging GmbH (2013) IF-MeasureSuite Version 5.1 User Manual. Alicona Imaging GmbH, Graz

[35] Hurtado Molina EE (2023) False Brinelling and Fretting Wear in Wind Turbine Pitch Bearings. PhD thesis, University of Sheffield, Sheffield. https://etheses.whiterose.ac.uk/id/eprint/32550/. Accessed 13 September 2026

[36] Rebegea SA (2018) Nanosecond Laser Ablation of Thin Film Material Libraries. PhD thesis, University of Birmingham, Birmingham. https://etheses.bham.ac.uk/id/eprint/8555/. Accessed 16 September 2026

[37] Haddad M, Zitoune R, Eyma F, Castanié B (2013) Machinability and surface quality during high speed trimming of multi directional CFRP. International Journal of Machining and Machinability of Materials 13(2–3):289–310. https://doi.org/10.1504/IJMMM.2013.053229

[38] Seeholzer L, Krammer T, Saeedi P, Wegener K (2022) Analytical model for predicting tool wear in orthogonal machining of unidirectional carbon fibre reinforced polymer (CFRP). The International Journal of Advanced Manufacturing Technology 119(11–12):7259–7289. https://doi.org/10.1007/s00170-021-08322-6

[39] Bi G, Wang F, Fu R, Chen P (2022) Wear characteristics of multi-tooth milling cutter in milling CFRP and its impact on machining performance. Journal of Manufacturing Processes 81:580–593. https://doi.org/10.1016/j.jmapro.2022.07.008

Statements and Declarations

Funding

The authors declare that no funds, grants, or other support were received during the preparation of this manuscript.

Competing Interests

The authors have no relevant financial or non-financial interests to disclose.

Author Contributions

Anh Tuan Dang: Conceptualization, Methodology, Investigation, Data curation, Formal analysis, Visualization, Writing – original draft.
Van Chec Nguyen: Investigation, Validation, Writing – review & editing.
Gunasilan Manar: Validation, Resources, Writing – review & editing.
Dinh Ngoc Nguyen: Conceptualization, Methodology, Supervision, Project administration, Writing – review & editing.

Data Availability

The data supporting the findings of this study are available from the corresponding author upon reasonable request.

Supplementary Files

This is a list of supplementary files associated with this preprint. Click to download.

- CFRPGraphicalAbstract.png